

Experimental and computational studies of piano hammers

Anatoli Stulov

Centre for Nonlinear Studies, Institute of Cybernetics, at Tallinn Technical University, 12618, Tallinn, Estonia, stulov@ioc.ee

Abstract

A piano hammer testing device, designed for measuring the force and compression histories during a hammer strike on a rigid surface, is described. The device was used in recording dynamic force-compression characteristics of piano hammers. The measurements were compared with simulations obtained with a hysteretic (hereditary) model of felt hammers. The elastic and hereditary parameters in the model were determined for various hammers by matching the simulated force-compression characteristics to the measured data. A good agreement with the theoretical model was obtained. The influence of string dummies of different diameters on the hammer parameters was examined, as well as the influence of the air humidity. Hammers from different manufacturers were compared, and the changes in the hammer parameters during the voicing process discussed. The continuous variation in the hammer parameters across the compass of the piano were determined for a set of hammers.

PACS: 43.75.Mn, 43.75.Yy

1. Introduction

The development of the piano over several centuries has resulted in a complex instrument. The hammers and strings form the basic sound-generating elements of the piano, and a number of studies have been devoted to the hammer-string interaction. Good reviews of previous work are given by Hall [1], Suzuki and Nakamura [2], and Fletcher and Rossing [3]. More recent publications include a tutorial by Conklin [4], and interesting work on piano hammers by Russell and Rossing [5], and Giordano et al [6,7]. The focus of these studies has been on improving mathematical models of piano hammers, and advancing the experimental investigations of the interaction between the hammer and the vibrating string. Most studies have used a power law for the piano hammer model, without considering the hysteresis effects.

To our knowledge there is only one study (Yanagisawa and Nakamura [8]), which reports direct experimental research on the compression characteristics of piano hammers. These important experiments demonstrated the main dynamical features of piano hammers: (a) the nonlinearity of the force-compression characteristics of the hammer, (b) the strong dependence of the hammer velocity on the slope of the loading curve, and (c) the significant influence of hysteresis, i.e. the loading and unloading processes of the hammer felt are not identical. It was also shown for the first time that the hammer felt is still deformed after the acting force has ceased.

An experimental investigation of the compression characteristics of piano hammers, carried out almost 20 years later [6], aimed at verifying previously presented hammer compression models in the form of a power-law dependence. An interesting contribution to the force-compression characteristic, attributed to the bending of the hammer shank, was reported. The results were, however, somewhat ambiguous as a direct measurement of the hammer compression was not provided in the experiments. Instead, an accelerometer mounted on the wooden core of the hammer head was used, and the hammer felt compression was obtained by integrating the acceleration twice. The striking velocity of the hammer, which is an independent value in the experiment, was also determined by integration. Such an approach may lead to erroneous conclusions about the form of the force-compression characteristics of the hammers tested.

A new, nonlinear, hysteretic model of the piano hammer that is in a good agreement with the experimental data presented in [8] has been described by the present author [9]. The model is based on the assumption that the hammer felt (made of wool) is a microstructural material possessing history-dependent properties, i.e. a material with memory. In addition to the elastic parameters, two hereditary parameters (hereditary amplitude and relaxation time) are introduced in order to describe the hysteretic behavior of the hammer.

The aims of the present study are to (a) collect new experimental data on piano hammers for comparison with the hysteretic model described in [9], (b) compare the interaction of the hammer with string dummies of different diameters, (c) compare piano hammers produced by different manufacturers, (d) investigate the influence of air humidity and voicing on the hammer parameters, and (e) estimate the continuous variation in the hammer parameters across the compass of the piano.

A special piano hammer testing device was designed for the experiments. Descriptions of the device, calibration procedures, and accuracy of measurements are provided in Sections 2-3. A procedure for determining the hammer parameters using numerical simulation is described in Section 4, and the experiments investigating topics (a) through (e) above are reported in Sections 5-9. The interaction of the hammer with a vibrating string will be described in forthcoming papers (see also [10,11]).

2. Hammer testing device

The hammer testing device is shown in Fig. 1 (a). The main physical principle of the device is to use the force of gravity for the hammer movement. The hammer is not launched by a key action as in a piano, but falls down freely. This principle makes it possible to eliminate the influence of the bending of the shank on the measurements. The shank was made of a rigid titanium tube, and therefore any bending of the shank due to inertial forces is extremely small (see Sect. 3.2).

The design provides hammer velocities in the range from 0.3 to 1.5 m/s. This range does not cover the range of hammer velocities in real playing, which can be up to 5 m/s in grand pianos. However, here the hammer does not strike a flexible string but a rigid object, and therefore the compression force and the hammer felt deformation will reach high values for lower velocities. Moreover, our experiments show that the hammer parameters are essentially independent of the hammer velocity, and therefore a maximum value of 1.5 m/s is not a strong limitation.

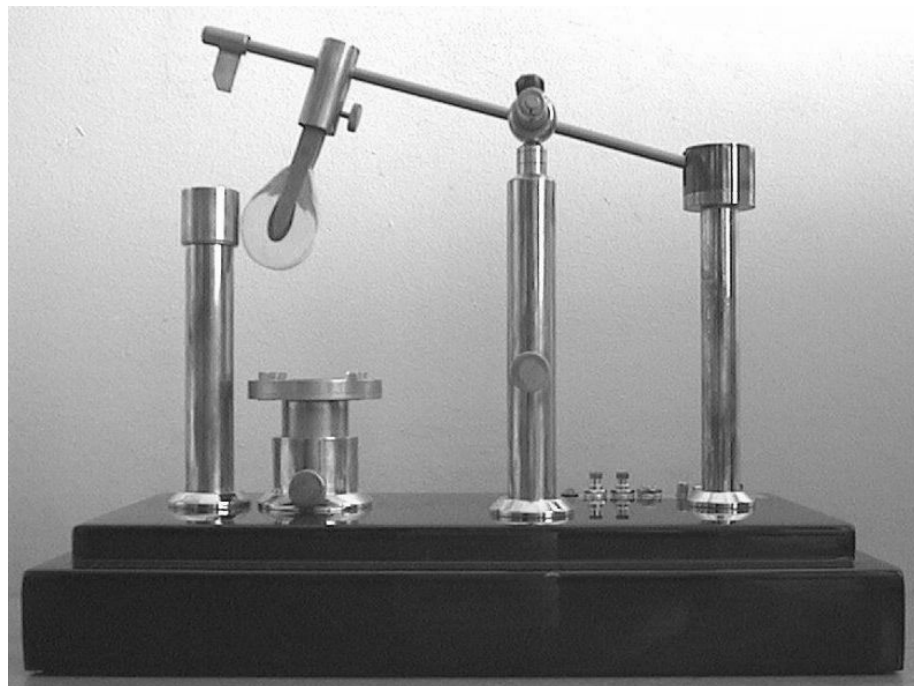


Fig. 1 (a). Hammer testing device.

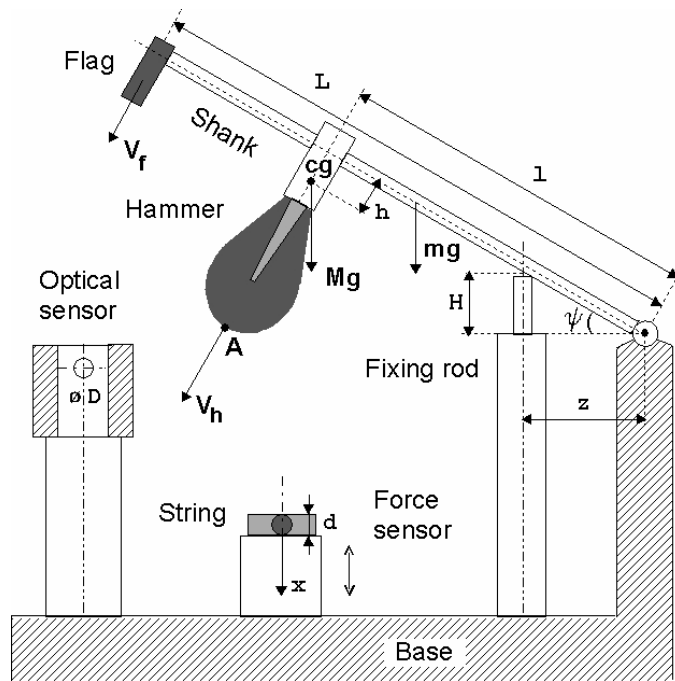


Fig. 1 (b). Functional scheme of the hammer testing device.

The functional scheme of the device is shown in Fig. 1 (b). The fixing rod determines the initial position of the hammer. By changing the altitude H over the horizontal level the angle ψ can be varied, and thus the velocity of the hammer at impact (*striking velocity*). On pulling a trigger the hammer falls down and strikes a flat facing on a force sensor. Alternatively, a steel dummy, simulating a piece of string, can be attached to the force sensor. The base of the force sensor is adjustable in the vertical direction in order to provide a horizontal positioning of the shank at the strike ($\psi = 0$) for all sizes and types of hammers.

An infrared optical system was developed for registration of the hammer compression. The displacement of a flag placed at the end of the shank is measured by the change in light intensity as the flag passes through the detector area of a fixed optical sensor. This enables the determination of the position of point A on the hammer by simple geometrical relations. The momentary hammer compression is defined as the difference between the initial hammer position just before the strike and the current position. The general design of the hammer testing device is very robust, the weight of the base plate being 4 kg.

The analogue signals from the force and optical sensors are converted into two sets of data by a 12-bit digital signal processor with nominal input range 0 - 5 V (resolution 1.2 mV) and throughput rate 285 kHz per channel (sampling period 7 μ s). The device is controlled by a PC in which the force and displacement signals are stored. The calibration of the force and displacement sensors as well as the determination of striking velocity are described in the following sections.

The piano hammer testing device is not intended to be a control-and-measuring gauge for determination of piano hammer parameters in manufacturing. It was designed for the purpose of laboratory testing of hammers by simultaneously recording force and hammer deformation during a strike in order to obtain force-compression characteristics.

3. Calibration

3.1 Force sensor

A custom-made piezoelectric force sensor (diameter 20 mm) with a thin, flat facing was designed for the hammer testing device. The sensor was connected to a voltage amplifier. A typical output signal directly from the sensor during a hammer strike as registered by a digital oscilloscope is shown in Fig. 2, and compared with the output of the amplifier.

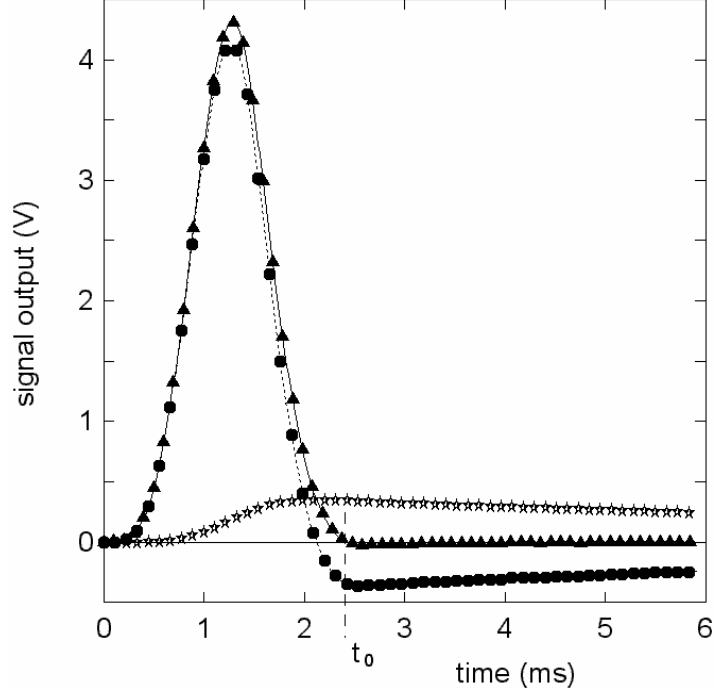


Fig. 2. Measured and corrected signals from the force sensor; Oscilloscope signal from the piezoelectric sensor (solid line), output from voltage amplifier (dots), corrected force signal (triangles), and correction term (asterisks). The end of the force pulse is indicated by t_0 (see text).

The output signal from the amplifier shows a undershoot due to a limited input impedance. The recorded signal was corrected numerically in the computer according to

$$U_0 = U_r + C_1 \frac{dU_r}{dt} + C_2 \int_0^t U_r dt . \quad (1)$$

Here U_0 is the corrected signal and U_r is the registered signal. The constants C_1 and C_2 were found numerically by introducing the constraint that the signal should reach zero level after the end of the force pulse. It emerged that only the third term contributed to the correction term ($C_1 = 0$). The correction term compensates for a high-pass RC circuit with time constant $1/C_2 = 0.95$ ms (cut-off frequency 170 Hz). The circuit is made up of the input resistance of the amplifier in combination with the capacitances of the sensor, cable, and amplifier. The corrected output signal U_0 from the amplifier traced the signal from the sensor accurately (see Fig. 2). The correction term is also shown.

The variation in zero level of the force signal after the end of a strike due to noise did not exceed 0.01 V, which corresponds to a force less than 0.1 N. This value was taken as the threshold level for determining the end of the force pulse t_0 (see Fig. 2). The same criterion was applied for determining the onset of the force pulse. The error in the determination of the duration of contact (as defined by the threshold values) did not exceed 2-3 samples ($< 21 \mu\text{s}$).

The force sensor was calibrated by dropping a loose hammer head made of hard wood (not attached to the titanium shank) on the facing. A piece of thin sticky tape prevented the hammer head from bouncing up from the sensor. Integrating the force signal over the contact time gives the mechanical impulse P_0 of the hammer in electrical units (Vs). The hammer mass m_0 and dropping altitude H_0 are known, and therefore the impulse M_0 in mechanical units (kgm/s) is also known. The force calibration coefficient K_f is given by

$$K_f P_0 = M_0 = m_0 V_h = m_0 \sqrt{2gH_0} \quad , \quad (2)$$

where V_h is the hammer velocity at impact, and g the gravity constant. The value of the calibration coefficient, 11.5 ± 0.7 N/V ($\pm 6\%$), was found by averaging the results of a series of measurements with different dropping altitudes H_0 . The main cause of the spread in calibration data was due to the fact that the hammer did not always strike precisely at the center of the force sensor. The value of the force calibration coefficient changed when string dummies were attached (see Sect. 5).

3.2 Hammer position sensor

The optical sensor, used for the hammer compression measurements, must be a more precise instrument than the force sensor. The history of the compression of the felt during the loading and unloading of the hammer reflects the hysteresis of the process, and so the device must be capable of giving accurate measurements of even small hammer deformations. The optical sensor has two outputs; one DC output used for static measurements, and a more sensitive AC output, used for dynamical measurements.

The calibration of the AC channel output was carried out using the same custom-made hammer head of wood as above, now fastened to the titanium shank. The base of the force sensor was lowered so that the flag on the shank could pass the optical sensor entirely before the hammer touched the force sensor. During the free fall of the hammer, the aperture is successively closed. By recording the output signal U_{AC} , we can find the time t_I during which the hammer passes through the aperture. The moments when the flag entered and closed the aperture, respectively, were identified in U_{AC} by comparison with the known static values for completely open and closed aperture.

The working range of the aperture d is a constant value determined from static measurements using a dial gauge, $d = 3.05 \pm 0.01$ mm. The frictional torque in the hammer testing device was checked to be very small and may be neglected here. Therefore, while falling the short distance corresponding to the width of the aperture only the force of gravity changes the hammer velocity. Thus, we can determine the hammer position X during the passage of the aperture from

$$X = V_1 t + \frac{1}{2} g t^2 \quad . \quad (3)$$

Using the boundary condition $X = d$ at $t = t_I$ we have the hammer velocity V_1 at $t = 0$

$$V_1 = \frac{d}{t_1} - \frac{1}{2} g t_1 \quad . \quad (4)$$

Equation 4 enables us to find the hammer velocity V_I at the moment when the flag reaches the aperture by measuring t_I .¹ This is the first step in deriving the dynamical calibration curve for hammer position.

The value of t_I can be obtained with a maximum error of two time steps (± 0.014 ms), one at the beginning and one at the end of the passage of the flag through the aperture. Even for the lowest hammer velocity used (about 0.4 m/s), the rate of change in voltage from the optical sensor exceeded the resolution limit (1.2 mV/time step) at the moments when the flag entered and closed the aperture, respectively.

¹ Note that when making the actual measurements in the hammer tests a different procedure of determining the hammer velocity just before the strike is used, see Sections 3.3 and 4. In the tests, the optical system is used to measure the compression of the hammer and the hammer does not fall freely during the passage of the flag through the aperture.

The small measurement error in the determination of t_I gives a high accuracy in the velocity determination. For example, if we find $t_I = 3.430 \pm 0.014$ ms (which corresponds to a hammer velocity in the mid range for the testing device), then according to Eq. (4) we have $V_I = 0.872 \pm 0.007$ m/s (± 0.8 %). The relative error in V_I did not exceed 1% for any velocity.

The second step in the hammer position calibration is to transform the recorded signal from the optical sensor (voltage vs. time) to a function of the current hammer position X , using Eq. (3) and the calculated value of V_I from Eq. (4). The calibration procedure was repeated for three hammer velocities, giving the dynamical calibration curve in Fig. 3.

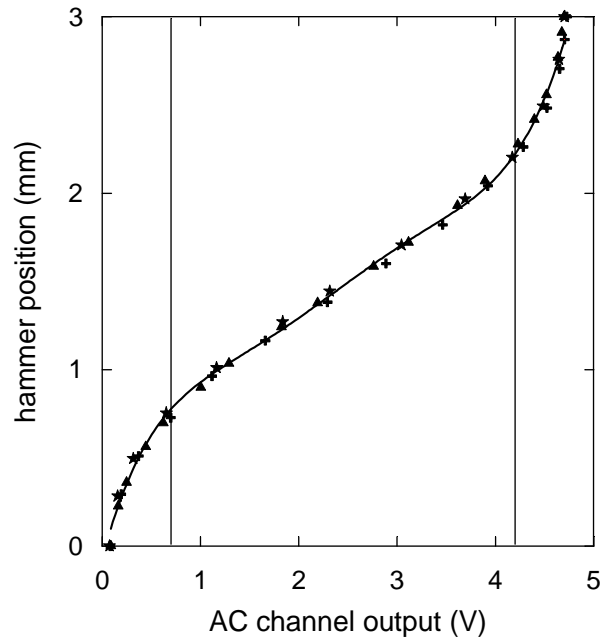


Fig. 3. Dynamical calibration curve showing hammer position vs. output voltage from the optical sensor. The zero level in hammer position corresponds to a horizontal position of the hammer (the flag reaches the aperture of the optical sensor). The data points correspond to hammer velocities of 0.672, 0.872, and 1.071 m/s. The solid line is a polynomial fit to the data. Only the middle section between the dashed lines was used in the measurements on hammers.

Three sets of data, obtained for hammer velocities of 0.672, 0.872 and 1.071 m/s are displayed. The solid line is a 5th-order polynomial fit of 42 points of experimental data obtained using a least-squares method. This polynomial defines the dynamical calibration curve for hammer position. In order to increase the measurement accuracy only the middle, almost linear, section of the working range was used in the hammer tests. This limited the maximum measuring range for hammer compression to about 1.5 mm.

In order arrive at an estimate of the resulting uncertainty in the determination of the hammer compression, a regression line fitted to the middle section of the calibration curve was computed together with the associated 95%-confidence interval. As the hammer compression is obtained as a difference between two readings only the uncertainty in the slope of the regression line is of interest. The slope estimated by the confidence interval was 0.38 ± 0.012 mm/V ($\pm 3\%$). For strong blows with the testing device, giving a maximum hammer compression of about 1 mm, the absolute error in the compression measurement was thus less than 0.06 mm. Note that the regression line gives an upper estimate of the error in the compression measurements. The actual calibration curve, defined by the polynomial fit, gives a better performance.

The error in the compression measurements due to the quantization of the output voltage from the optical detector was very small, far less than the errors introduced by the uncertainty in the calibration curve. The nominal resolution in the measurement of hammer position was $1.2 \text{ mV} \cdot 0.38 \text{ mm/V} = 0.0005 \text{ mm}$ for the middle section of the calibration curve.

A high accuracy in the compression measurements can be achieved only with a very rigid configuration of flag, shank, and hammer. In particular the bending of the left part of the shank is important as the flag is placed at this end (see Fig. 1). The shank bending due to inertial forces as the hammer strikes the force sensor can easily be estimated. A maximum value of the hammer deceleration ($1600 - 2000 \text{ m/s}^2$) was observed for the rigid hammer made of wood. A numerical estimation of the maximum flag displacement due to the bending of the titanium tube for this case yields a value of 0.006 mm .

The calculated maximum bending of the titanium tube was verified experimentally. With the wooden hammer resting on the force sensor, the initial position at contact was measured by registration of the DC-coupled position signal U_{DC} . Then the same signal was registered during a hammer strike. Only for very hard strikes a difference in hammer position before and during contact was observed, reflecting the combined effects of bending of the titanium tube, and compression of the wooden hammer and force sensor. For the hardest possible blow with the device (at the maximum limit of the force sensor) this difference reached a value of 0.01 mm . The deceleration of a normal felt hammer is at least several times less than that of the wooden hammer, and thus the influence of the bending of the titanium shank can be considered as negligible.

3.3 Presetting the hammer striking velocity

We know that piano hammers possess hysteresis, which means that they are very sensitive to the rate of loading. For this reason the velocity of the hammer at impact (striking velocity V_h) is an important parameter in a determination of hammer properties, and it must be known with a rather high accuracy. The exact measurement of the striking velocity in each hammer test relied on a numerical method, integrated with the processing of the recorded compression data (see Sect. 4). In the experiments, we must, however, be able to preset an approximate striking velocity on the testing device. This was done by setting the initial altitude H relative to the horizontal position of the shank at the strike (see Fig. 1 (b)).

Thin strokes with a spacing of 1 mm were marked on the fixing rod for this purpose. By letting the hammer fall freely and using the method of velocity determination described in Sect.3.2, a simple empirical relation to calculate V_h [m/s] from the altitude H [mm] was derived

$$V_h = -29 \cdot 10^{-6} H^2 + 0.2\sqrt{H} . \quad (5)$$

Using this formula the geometry of the moving parts of the device and additional forces, such as friction and air drag, need not to be taken into consideration, as all is included in Equation (5). The instrumental error of the altitude determination was rather large, $\Delta H \approx 0.5 \text{ mm}$. The corresponding maximum error in the preset striking velocities did, however, not exceed 0.025 m/s (6%), which occurred for the case $H = 4 \text{ mm}$, giving $V_h = 0.40 \text{ m/s}$. Nevertheless, Eq. (5) was used only to preset an approximate target value of the striking velocity.

4. Numerical simulation of hammer tests

The following section presents a systematic approach for determining the hammer parameters, using measured force-compression characteristics from the hammer testing device and a theoretical model of the hysteretic piano hammer. The model was derived in [9] in the form

$$F(u(t)) = F_0 \left[u^p(t) - \frac{\varepsilon}{\tau_0} \int_0^t u^p(\xi) \exp\left(\frac{\xi-t}{\tau_0}\right) d\xi \right] . \quad (6)$$

Here $F(u)$ is the force exerted by the hammer and u is the hammer compression. The hammer stiffness F_0 and compliance nonlinearity exponent p are the elastic parameters of the hammer, and hereditary amplitude constant ε and relaxation time τ_0 are the hereditary parameters. According to this model, a real piano hammer possesses history-dependent properties, or in other words, it is made of a material with memory.

The hammer parameters may be obtained from numerical simulations of the dynamical tests. This procedure, previously presented in [9,12], is based on a mathematical model of the experiments with the piano hammer testing device. In short, the impact of the hammer can be described by the equation of motion

$$m_0 \frac{d^2 u}{dt^2} + F(u) = 0 , \quad (7)$$

with the initial conditions

$$u(0) = 0, \quad \frac{du}{dt}(0) = V_h . \quad (8)$$

Here, as above, m_0 and V_h are the hammer mass and the striking velocity respectively, and $F(u)$ is defined by Eq. (6).

Initially unknown, the values of the hammer parameters are obtained by iterated numerical simulations. The force-compression characteristic $F(u)$ is first calculated from Eq. (7) using plausible initial values of the parameters. The simulations are then run repeatedly, each time with manually adjusted parameter values, until the model prediction is in good agreement with the experimental data.

Let us consider this procedure in an example with a hammer manufactured by Renner (key number $N = 14$, note $Bb_1 = 58.3$ Hz). A test is run with the hammer testing device. The signal from the force sensor is corrected according to Eq. (1) and converted to force units using the calibration coefficient K_f . The hammer compression history is obtained from the hammer position signal, using the dynamical calibration curve in Fig. 3. The force and compression histories for three tests with different hammer velocities are presented in Figure 4(a) and (b).

In Fig. 4(c) the force-compression characteristics, obtained by combining the force and compression histories, are displayed. The arrows show the directions of the compression and decompression branches. A significant influence of hysteresis can clearly be seen in the hammer characteristics (the loading and unloading of the hammer do not follow the same path). Moreover, the slope of the force-compression characteristics increases with increasing hammer velocity, just like the model of the hysteretic hammer predicts.

In order to provide a numerical simulation of the experimental data, the values of the striking velocity V_h must be known. The altitude H in the series of experiments in Fig. 4 was equal to 47, 26, and 14 mm. According to Eq. (5) the striking velocities were 1.31, 1.00, and 0.74 m/s, respectively. The accuracy in the preset striking velocities was ± 0.01 m/s in all three cases.

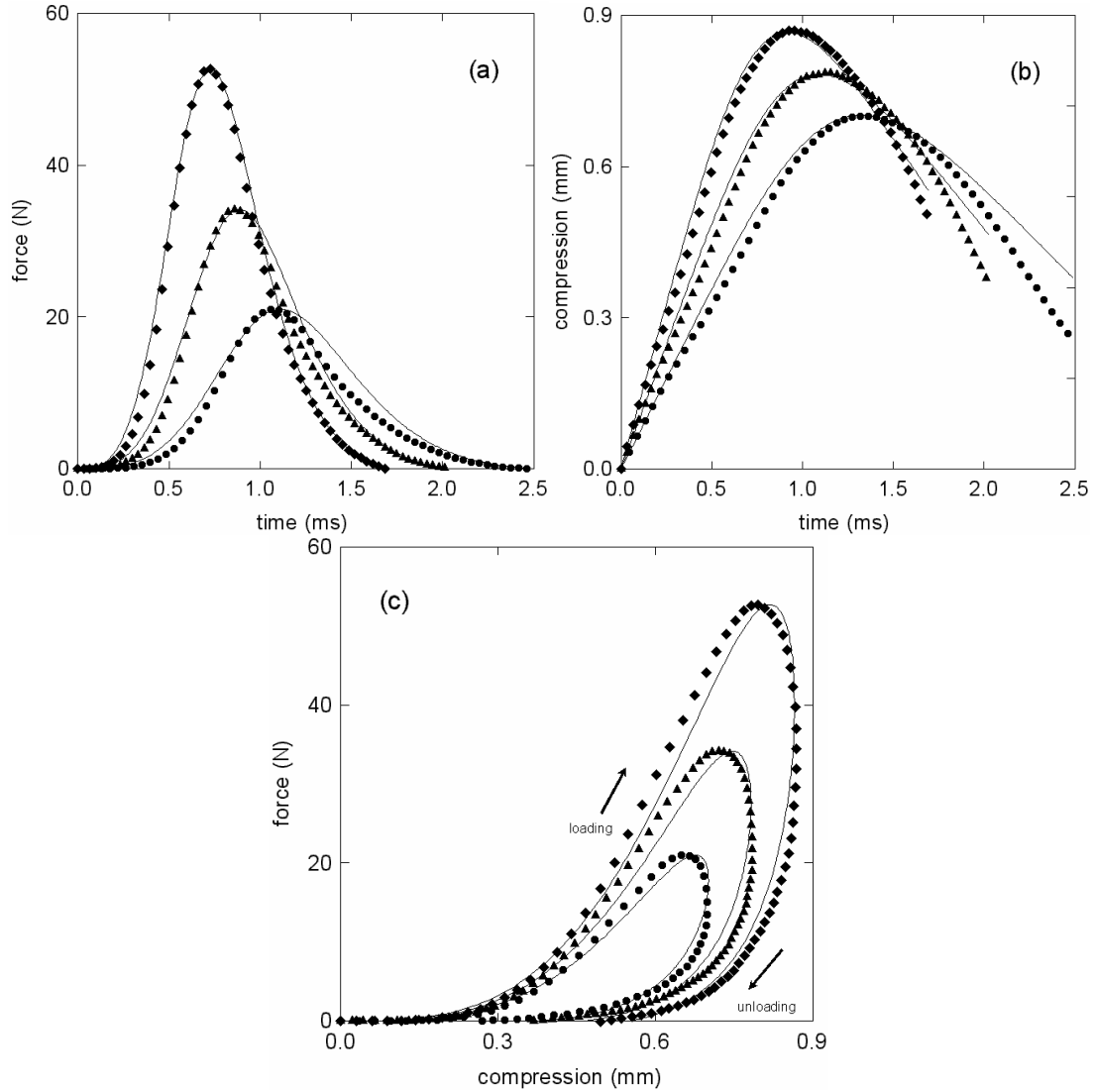


Fig. 4. Comparison of measured data and numerical simulations in a test of a Renner hammer ($N = 14$, note $Bb_1 = 58.3$ Hz) showing (a) force histories (b) compression histories, and (c) force-compression characteristics. The arrows show the directions of the compression and decompression branches. The symbols denote measured data for hammer striking velocities 1.31 m/s (*diamonds*), 1.00 m/s (*triangles*), and 0.74 m/s (*bullets*). The solid lines are the numerically simulated curves.

However, the numerical simulations of the hammer tests offer a more practical and accurate method of determining the striking velocity of the hammer. According to the second initial condition (Eq. 8), the time derivative of the compression at the beginning of the process is equal to the striking velocity. Further, Figure 4(b) shows that the initial parts of the compression histories are approximately linear for a rather long time. This fact is used in the simulation program, which automatically provides an approximation of the first 20 points ($0 < t < 0.2$ ms) of the compression data by a linear function using a least-squares method [13]. The coefficient of this fit is the striking velocity of the hammer. The values of V_h in Fig. 4 determined by this method are 1.306, 0.995, and 0.740 m/s, respectively. These values are very close to the preset values of 1.31, 1.00, and 0.74 m/s.

The accuracy implied by the curve-fitting method is very high. The squared linear regression coefficients R^2 , indicating how well compression data is explained by a best-fit line, were above 0.999 in all three cases. However, the dynamical position calibration curve, on which the compression data are based, is not as accurate and reduces the accuracy in the determination of the striking velocity to ± 0.01 m/s. More importantly, we do not need such a high accuracy. Due to a trade-off procedure in the determination of the hammer parameters in which several criteria are considered (see below), an

accuracy of ± 0.03 m/s was estimated to be sufficient for hammer testing purposes. This accuracy in striking velocity can easily be reached by the described numerical method (and in fact even by a careful presetting of the altitude H).

In the numerical simulations, the parameters are chosen such that a good agreement with the experimental data is obtained simultaneously for both force and compression histories. This means that not only similar shapes and magnitudes of the simulated and experimental curves should be obtained, but also that the duration of the calculated contact time should be close to the experimental value. The contact time was here considered as the primary criterion, because the contact duration is an objective and well-defined quantity to measure. The hammer parameters were chosen in such a way that the difference between the measured and simulated contact times was reduced to less than 0.01 ms, while reaching an approximate matching of maximum values of force and hammer compression simultaneously. Visual inspection of the simulated curves in Fig. 4 shows that it was possible to reach a good match of all three quantities simultaneously.

All simulated curves in Fig. 4 were obtained using only one combination of hammer parameters: $F_0 = 8800$ N/mm^p; $p = 3.95$; $\varepsilon = 0.992$; $\tau_0 = 2.0$ μ s. Only the value of the hammer striking velocity was varied. The best fit was achieved for striking velocities of 1.32, 0.99, and 0.72 m/s, respectively. These values are very close to the striking velocities determined in the experiment, in fact within the limits of measurement accuracy (± 0.03 m/s). The estimated uncertainty in determining the hammer parameters was approximately $\pm 1\%$ for F_0 , ± 0.02 for p , ± 0.002 for ε , and ± 0.1 μ s for τ_0 .

The accuracy in determining the hammer stiffness F_0 and the other hammer parameters is not primarily related to the accuracy of the hammer testing device. The main cause of the uncertainty in the estimation of the hammer parameters is connected with the trade-off between the parameter values during the matching of the simulations to the measured data (in which three quantities are matched simultaneously).

The successful matching demonstrated in Fig. 4 is an important result. The three sets of data, corresponding to three different striking velocities, were matched accurately by simulations using the *same* set of hammer parameters. This result indicates that the hysteretic hammer model gives a good description of real piano hammers. For a single force-compression characteristic, an almost perfect match between simulated and experimental curves can be achieved.

5. Influence of string diameter

When the hammer strikes a string instead of a flat surface, it is obvious that the conditions of the strike are not quite the same. A thin string penetrates into the hammer more easily than a thick string or a flat facing, as it does not directly engage the felt across the full width of the hammer. On the other hand, the outer parts of the hammer, which are brought into play by a thick string, are softer and may compress easier than the deeper layers at the center. For these reasons the changes in the hammer-string interactions for different striking conditions are not evident.

A set of measurements was performed to clarify whether the hammer parameters depend on the diameter d of the struck string or not. The results obtained with the normal flat facing were compared with the results produced by striking different samples of steel cylinders (string dummies) placed on the force sensor. The force-compression characteristics measured for three diameters of string dummies, all at a striking velocity $V_h = 1.31$ m/s ($H = 47$ mm), are presented in Fig. 5. The force calibration coefficient K_f had to be adjusted for the differences in loading of the force sensor as the mass of the dummy reduced the sensitivity. This was done using the force calibration technique described in Sect. 3.1.

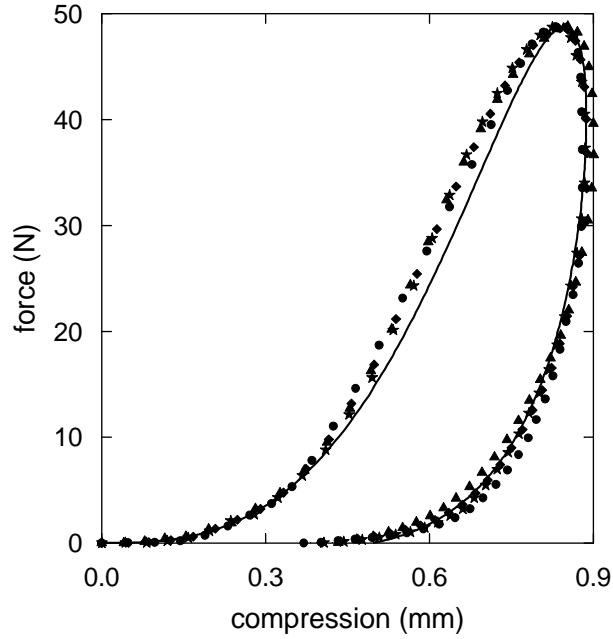


Fig. 5. Influence of the string diameter on the force-compression characteristics (Renner hammer, $N = 16$, note $C_2 = 65.4$ Hz). Measured data for flat facing (*diamonds*), and string dummies with diameter $d = 1$ mm (*triangles*), 2 mm (*stars*), and 5 mm (*bullets*). The force calibration coefficient K_f was adjusted to each case because of the differences in loading of the force sensor by the dummies. The solid line is the numerically simulated curve.

As seen in the figure, the data obtained with the flat facing and the three string dummies follow essentially the same curve. This result indicates that the process of the hammer-string interaction actually may depend very little on the diameter of the struck string.² In this respect, testing of hammers against a flat surface would give a fair approximation of the real conditions in a piano. The solid line in Fig. 5 is the simulated force-compression characteristic obtained for hammer parameters $F_0 = 7700$ N/mm^p, $p = 3.60$, $\varepsilon = 0.992$, $\tau_0 = 1.8$ μ s.

6. Comparison of hammers from different manufacturers

The next series of measurements was carried out in order to compare piano hammers from different manufacturers. Four brand-new (unvoiced) hammers with similar dimensions and masses ($m_0 = 9$ g ± 0.2 g) produced by *Abel*, *Imadegawa*, and *Renner* (*old* and *new* type), were chosen. The experimental data are compared in Fig. 6(a). The striking velocity was approximately equal to $V_h = 1.0$ m/s in all tests (see Table 1). All hammers fell from the same altitude in the testing device, and the small velocity differences were caused by differences in geometry, size, and mass of the hammers. The values of the hammer parameters obtained from the simulations are displayed in Table 1.

² The conclusion drawn in [10] about the influence of the string diameter on the hammer-string interaction may have been too strong. In that study the force calibration coefficient K_f was not adjusted for the difference in masses of the dummies.

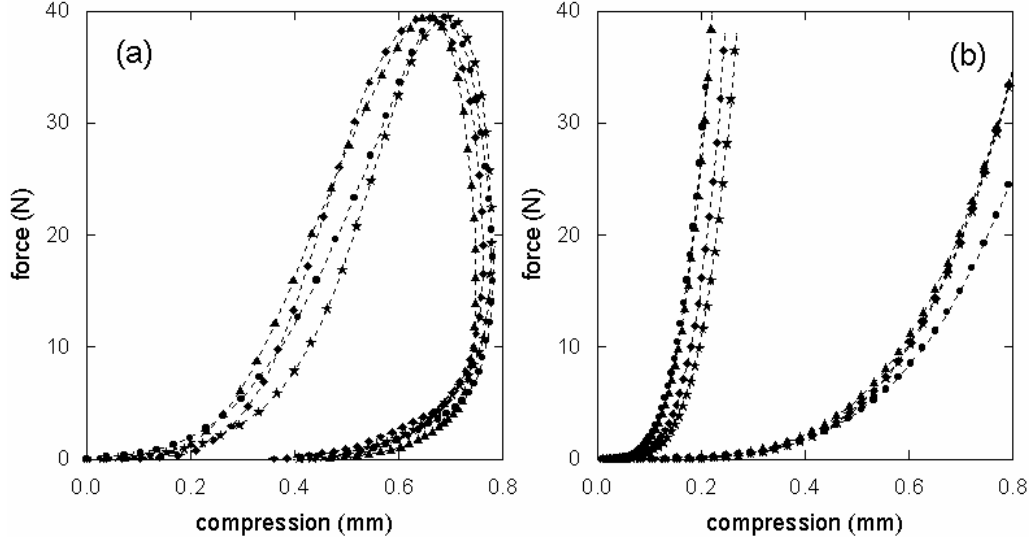


Fig. 6. Comparison of four new (unvoiced) hammers from different manufacturers (a) Experimentally measured force-compression characteristics; *Abel* (diamonds), *Imadegawa* (stars), and two *Renner* hammers, *old type* (triangles) and *new type* (bullets). (b) Calculated force-compression characteristics for very fast (instantaneous) compression (left branches) and slow (static) loading (right branches).

Quantity	Hammer type			
	<i>Abel</i>	<i>Old Renner</i>	<i>New Renner</i>	<i>Imadegawa</i>
F_0 (kN/mm ^p)	15.0	17.0	14.0	11.3
p	4.25	4.00	3.85	4.30
ε	0.994	0.995	0.995	0.992
τ_0 (μ s)	2.00	2.30	2.25	2.40
V_h (m/s)	1.05	1.08	1.10	1.04

Table 1. Numerically determined parameters of hammers from different manufacturers.

The results in Fig. 6 suggest that the differences in force-compression characteristics between (unvoiced) hammers from different manufacturers are not very significant. The force-compression characteristic of the new type of Renner hammer is less steep than for the old type, and the shape of the characteristic approaches that of the Imadegawa hammer. The old type of Renner hammer is more similar to the Abel hammer.

The similarity of piano hammers from different manufacturers may also be demonstrated in the frequency domain by calculating simulated string spectra. Stulov and Mägi [10] have shown that there were no specific distinctions between the hammers tested above in terms of string spectra. The largest difference in mode energy level was found for the 11th partial, reaching 3 dB.

The close agreement between the performance of hammers from different manufacturers can be demonstrated also in another way. In Fig. 6(b) the calculated force-compression characteristics of the same hammers as in Fig. 6(a) are presented for very fast and slow loading according to the theory in [9]. The left branches represent instantaneous loading given by

$$F(u(t)) = F_0 u^p(t), \quad (9)$$

and the right branches represent static loading given by

$$F(u(t)) = F_0 (1 - \varepsilon) u^p(t). \quad (10)$$

In spite of some differences in hammer stiffness F_0 , nonlinearity exponent p , and the hereditary amplitude ε (see Table 1), the resulting characteristics have a similar appearance.

It seems reasonable to conclude that piano hammers produced by different manufacturers have similar elastic features, their dynamical compression behavior is rather similar, and in the frequency domain the hammers are also almost indistinguishable (at least in simulations). This observation is somewhat surprising as a piano hammer is a rather complicated object. Modern piano hammers have a wooden core covered with one or two layers of compressed wool felt, whose stiffness increases from heavy bass hammers to light treble hammers. Felt made of wool has been used for piano hammer manufacturing for almost two hundred years. In spite of many attempts to develop a more suitable material, wool felt is still a unique coating material for piano hammers. One of the most important features of the hammer felt is the ability to provide much brighter sound for a strong *ff* impact than for a weak *pp* touch. This means that the felt stiffness increases with the rate of loading.

All hammer manufacturers use wool felt, but the preparation process of the felt as well as type of glue and impregnation compound and stretching and compressing of the felt strip over the wooden molding differ. All these technological procedures of hammer making are the know-how of each company. However, in spite of company secrets and long-term traditions, the dynamical features of hammers made by different manufacturers seem to be similar. The reason is without doubt the basic features of wool felt. It is well known, and further illustrated in the present study, that felt, being a microstructural material, possesses history-dependent properties. Due to these properties the dynamical behavior of contemporary piano hammers shows pronounced hysteresis in compression-expansion. In addition, the hammer stiffness is strongly dependent on the striking velocity. The ratio of the slopes of the force-compression characteristic for very slow (*pp*) and very fast loading (*ff*), respectively, which is defined by $\delta = 1 - \varepsilon$ [see Eqs. (9) and (10)], can reach 0.003 for treble hammers. At present it seems that only wool felt can provide the range in volume and quality of sound pianists demand in performance.

7. Influence of air humidity

The negative effect of high air humidity on the sound quality of pianos is well known. The next series of measurements was undertaken to investigate the influence of changes in humidity on the hammer parameters. A Renner hammer of the new type ($N = 20$, note $E_2 = 82.4$ Hz) was tested for this purpose. The experiment was run in a normal laboratory room when the humidity was suitable for the measurements. A simple type of psychrometer was used for determining the humidity. A very damp day was chosen for the measurements at a humidity of almost 100%. A very dry hammer (0% humidity) was prepared by heating. The hammer was held over a table lamp and exposed to the heat during a half an hour. The experimentally obtained force-compression characteristics for 0, 50, 70, 80, and 100% humidity are presented in Fig. 7. In this experiment the striking velocity was $V_h = 1.05$ m/s for all measurements.³ The values of the numerically determined parameters of the hammer are given in Table 2.

³ The hammer was not removed from the testing device between measurements, which gives a high reproducibility in striking velocity.

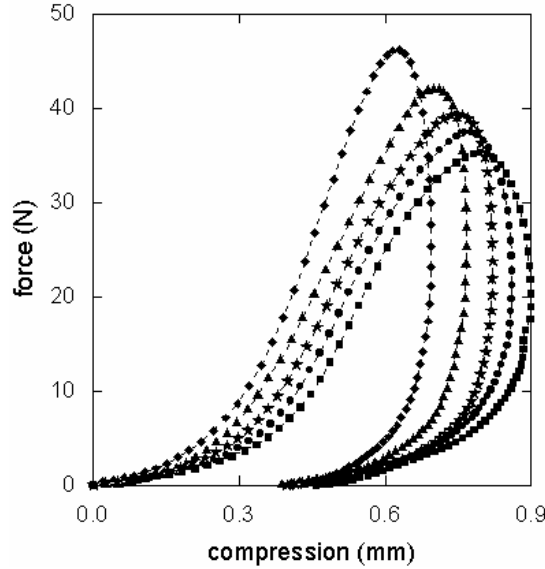


Fig. 7. Influence of air humidity. Measured force-compression characteristics of a hammer at 0% (*diamonds*), 50% (*triangles*), 70% (*stars*), 80% (*bullets*), and 100% (*squares*) humidity. Renner hammer, new type ($N = 20$, note $E_2 = 82.4$ Hz).

Quantity	Air humidity				
	0%	50%	70%	80%	100%
F_0 (kN/mm ^P)	16.0	10.0	7.4	5.8	4.7
p	3.72	3.72	3.72	3.72	3.72
ε	0.992	0.992	0.992	0.992	0.992
τ_0 (μ s)	2.7	2.8	2.9	3.0	3.1

Table 2. Numerically determined parameters of a Renner hammer of the new type ($N = 20$, note $E_2 = 82.4$ Hz) for different values of air humidity. $V_h = 1.05$ m/s for all measurements.

The results demonstrate clearly that the influence of the humidity on the hammer parameters is high; the hammer becomes softer with increasing humidity. The hammer stiffness F_0 may be reduced more than a factor of three, and the amplitude of the force-compression curves decreases. Both the reduction in hammer stiffness as well as the change in the relaxation constant τ_0 contribute to the significant differences between the force-compression characteristics for 0 and 100 % humidity, respectively. The increase in τ_0 with increasing humidity makes the area of the curves wider. As a result, the contact duration for the ‘damp’ hammer is approximately 10% longer than for the dry hammer. The two other hammer parameters p and ε appear to be less sensitive to air humidity. From a physical point of view, an increased moisture content does not change the structure of the felt, but instead it may make the wool fibres softer and act as a lubricant. The friction between the fibres may therefore be modified, resulting in a change in stiffness and affecting the relaxation constant.

8. Influence of voicing

An important method for changing the tonal quality of a piano tone is by *voicing*; a mechanical treatment of the piano hammer by needling. A ‘hard’ hammer can be softened by piercing it with needles. The qualitative influence of this procedure was investigated by testing a Renner hammer of the new type ($N = 37$, note $A_3 = 220$ Hz). A new, unvoiced hammer was run initially. Then the hammer was subjected to rather violent voicing by piercing with a needle 10 times down to 10 mm depth in the vicinity of the striking area. The striking velocity was $V_h = 1.1$ m/s for all cases.² The measured force-compression characteristics of the hammer before and after voicing are shown in Fig. 8. The curves show a strike of the hammer before voicing, the first and third strike after voicing,

respectively, and after a large number of strikes when the values of the hammer parameters have stabilized. A clear change in the force-compression characteristic before and after voicing is observed, followed by a recovery towards the initial characteristic after a large number of strikes.

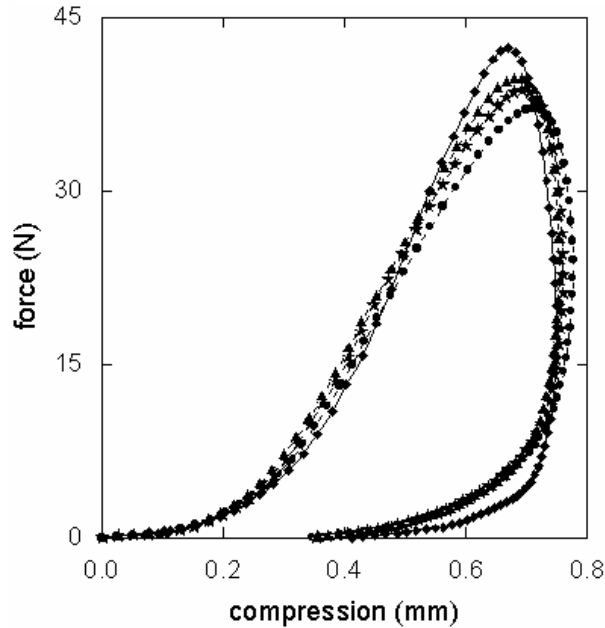


Fig. 8. Influence of voicing. Force-compression characteristics of a Renner hammer of the new type ($N = 37$, note $A_3 = 220$ Hz) before voicing (*diamonds*), the first strike after voicing (*bullets*), the third strike (*stars*), and after a large number of strikes (*triangles*).

Quantity	Case number			
	1	2	3	4
F_0 (kN/mm ^p)	32.0	19.0	23.0	25.5
p	4.0	3.74	3.74	3.74
ε	0.997	0.997	0.997	0.997
τ_0 (μ s)	1.0	1.5	1.3	1.2

Table 3. Numerically determined parameters of a Renner hammer of the new type ($N = 37$, note $A_3 = 220$ Hz); before voicing (case 1), the first strike after voicing (case 2), the third strike (case 3), and after a large number of strikes (case 4).

The values of the numerically determined parameters of the hammer are given in Table 3. The voicing reduces the hammer stiffness F_0 and increases the relaxation time τ_0 , but does not change the hereditary amplitude ε . The value of p decreases, but not by a significant amount.

The voicing process have a similar effect as an increase in air humidity, making the hammer softer. The reduction in hammer stiffness is of the same order of magnitude as for a variation in humidity of about 20%. The main and essential difference between these processes is that changes in the hammer parameters induced by variation in the humidity are reversible. The prolonged testing of the voiced hammer demonstrates that even after dozens of strikes and after many days, the initial characteristics of the hammer are not restored. It appears that the value of the nonlinearity exponent p reflects the character of the felt structure. This value is changed by needling and remains constant, indicating that the voicing process introduces irreversible changes in the structure of the felt.

9. Piano hammer set

Testing of a whole hammer set enables investigation of the continuous variation in hammer parameters over the compass of the piano. A set of recently produced unvoiced Abel hammers was measured for this purpose. The striking velocity V_h was not kept constant for all hammers. The hammer stiffness increases significantly with key (hammer) number N , so in order to obtain approximately the same maximum force for all hammers tested, the striking velocity was decreased systematically with increasing N . The dependence of the striking velocity on key number was approximately

$$V_h = 0.849 - 0.004N, \quad 1 \leq N \leq 88 \quad (11)$$

meaning that the velocity range covered in the measurements was rather large, decreasing from $V_h = 0.85$ m/s in the bass to 0.50 m/s in the treble.

The hammer masses of this set were approximated by

$$m_0 = 11.074 - 0.074N + 0.0001N^2, \quad 1 \leq N \leq 88 \quad (12)$$

The mass of hammer 1 (A_0) was 11.0 g and the mass of hammer 88 (C_8) 5.3 g.

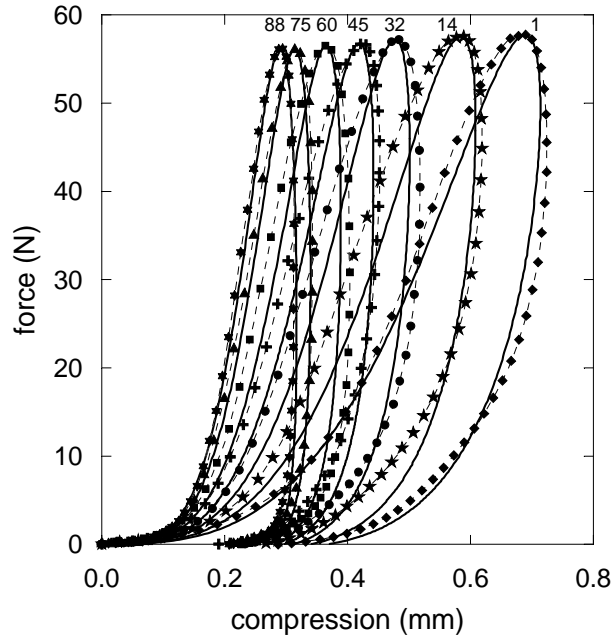


Fig. 9. Force-compression characteristics of seven hammers from a complete set of unvoiced Abel hammers (various symbols), and matched simulations (solid lines). The corresponding key numbers are shown above the curves.

The measured force-compression characteristics of seven hammers from the set are shown in Fig. 9. The measurements shown in the figure are typical samples of the observed trend. Continuous variations in the hammer parameters vs. key number were obtained by numerical simulation of the experimental data. A best match to the whole set of hammers was approximated using

$$p = 3.7 + 0.015N, \quad 3.72 \leq p \leq 4.98 \quad (13)$$

$$\varepsilon = 0.9894 + 0.000088N, \quad 0.9895 \leq \varepsilon \leq 0.9972 \quad (14)$$

$$\tau_0 = 2.72 - 0.02N + 0.00009N^2, \quad 1.65 \leq \tau_0 \leq 2.70 \text{ } [\mu\text{s}] \quad (15)$$

for hammer number $1 < N < 88$.

The simulated curves for the seven hammers in Fig 9 are depicted using solid lines. The agreement between the simulated curves and experimental data is rather good. The results indicate that the compliance nonlinearity exponent p and hereditary amplitude ε are linear functions of the key (hammer) number N for this set of hammers. The relaxation time τ_0 is a quadratic function of N . The hammer stiffness F_0 is a linear function on a logarithmic scale

$$F_0 = 15500 \exp(0.059 N), \quad 16440 \leq F_0 \leq 2787300. \quad (16)$$

the unit for F_0 being N/mm^p .

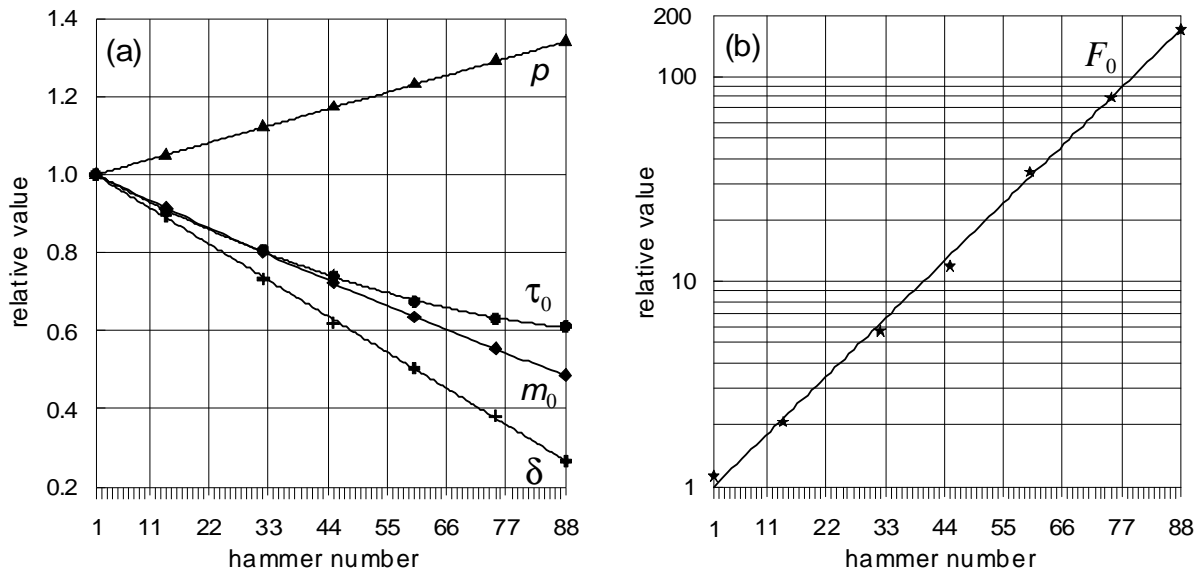


Fig. 10. Relative variation in hammer mass and compression parameters across the compass of the piano for a set of unvoiced Abel hammers. The values have been normalized relative to the lowest key ($N=1$); (a) compliance nonlinearity exponent p , relaxation time τ_0 , hammer mass m_0 , and $\delta = 1 - \varepsilon$ (where ε is hereditary amplitude); (b) hammer stiffness F_0 .

The relative variation in hammer mass and hammer parameters vs. key number N as defined by Equations (12) – (16) are presented in Fig. 10. The values have been normalized relative to the lowest key ($N=1$). Instead of the hereditary amplitude ε , the value of $\delta = 1 - \varepsilon$ is displayed here. The parameter δ shows the ratio of the slopes of the static and instantaneous force-compression characteristics (see Fig. 6(b) and Eqs. 9-10). As seen in Fig. 10, the hammer mass decreases by a factor two from bass to treble, while δ decreases by 70%, τ_0 decreases by 40%, and p increases by 35%. It is particularly interesting to note that the hammer stiffness F_0 increases exponentially by a factor 170 from bass to treble. This large change indicates that the hammer stiffness is the most influential parameter for the force-compression characteristic. The experience gained from the numerical matching of the measured compression characteristics supports this observation. The sensitivity of the model to changes in other parameters is approximately equal. However, it should be observed that the value of δ , being the difference between two almost equally large numbers (ε is always very close to unity), is particularly sensitive to matching errors.

For a high-quality set of unvoiced piano hammers, it seems plausible that the variation in hammer parameters with key number should be continuous and regular, as in Equations (13) - (16). The voicing procedure, which follows after installing the hammers in the piano, would then serve the purpose of adapting the individual hammers to relatively small key-to-key variations in the instrument. In contrast, if the measured values of the ‘raw,’ unvoiced hammers do not show a regular variation

with key number it would be tempting to conclude that the production process is not well controlled, and that the hammer set is not of good quality.

However, some precaution is necessary before drawing any firm conclusions. Not all of the measurements from the complete set of hammers could be used for determining the continuous variations in hammer parameters. The rejected hammers corresponded either to possible errors in measurements (strong variation in data), or to hammers with defects. The total number of hammers in the set was above 90 (88 plus extras), and the percentage of rejected data was nearly 20%. We hope that further experiments will clarify the origin of the data that had to be rejected.

10. Summary

A high precision device has been developed for dynamical testing of piano hammers. The experimental arrangement makes it possible to obtain force and compression histories during hammer strikes against a rigid surface. It was shown that the force-compression characteristics of the piano hammers tested could be successfully simulated by a hysteretic model. A main feature of the hammers is that the slope of the force-compression characteristic is strongly dependent on the rate of loading. Further, it has been shown that representative values of the hammer parameters can be obtained from measurements in which the hammer strikes a flat surface. The values of the hammer parameters are not strongly dependent upon the diameter of the struck object (string).

Comparison of four types of hammers from three manufacturers revealed that contemporary piano hammers have comparable elastic features. All of the hammers showed a hysteretic type of force-compression characteristic, and their dynamical behavior was rather similar. This phenomenon can be explained by the fact that all manufacturers use wool felt as coating material for the hammers. The wool felt seems to be a unique and indispensable material for piano hammers.

It was shown that the influence of air humidity on the hammer parameters is substantial. An increase in humidity makes the hammer softer. The voicing process affects the hammer in a similar way. The main difference between these effects is that changes in the hammer parameters induced by variation in the air humidity are reversible. In contrast, the procedure of piercing the felt with needles introduces irreversible changes in the structure of the felt.

The variation in hammer parameters vs. key number were derived from measurements on a complete set of unvoiced hammers. For the set of hammers tested the parameters changed smoothly over the compass of the piano.

The results obtained in this study can be applied to numerical simulations of string vibrations and spectra. They may also be useful for piano scale design and in the development of the hammer manufacturing process. Further investigations of the hammer-string interaction in the frequency domain may emphasize the significant hysteretic features of piano hammers. This topic will be examined in forthcoming studies.

Acknowledgments

The author is grateful to Professor Jüri Engelbrecht for many helpful discussions. Thanks also to the anonymous reviewers and Anders Askenfelt who provided constructive review and helpful comments on an earlier version of this paper. This project was supported by Estonian Science Foundation, Estonian Innovation Fund and Tallinn Grand Piano Factory.

References

- [1] D. E. Hall, "Piano string excitation III: General solution for a soft narrow hammer," *J. Acoust. Soc. Am.* **81**, 547-555, (1987).
- [2] H. Suzuki and I. Nakamura, "Acoustics of pianos," *Appl. Acoustics*, **30**, 147-205, (1990).
- [3] Fletcher, N. H. & Rossing, T. D., *The Physics of Musical Instruments*, Springer-Verlag (New York, 1991).
- [4] H. A. Conklin, Jr., "Design and tone in the mechanoacoustic piano. Part I. Piano hammers and tonal effects," *J. Acoust. Soc. Amer.* **99**, 3286-3296, (1996).
- [5] D. Russell and T. Rossing, "Testing the nonlinearity of piano hammers using residual shock spectra," *Acustica-Acta Acustica* **84**, 967-975, (1998).
- [6] N. Giordano and J. P. Winans II, "Piano hammers and their force compression characteristics: Does a power law make sense?," *J. Acoust. Soc. Am.* **107**, 2248-2255, (2000).
- [7] N. Giordano and J. P. Millis, "Hysteretic behavior of piano hammers," *Proc. of the International Symposium on Musical Acoustics (ISMA'2001)*, September 10-14, 2001 Perugia, Italy, Vol. 1, 237-240, (2001).
- [8] T. Yanagisawa and K. Nakamura, "Dynamic compression characteristics of piano hammer," *Transactions of Musical Acoustics Technical Group Meeting of the Acoustic Society of Japan* **1**, 14-18, (1982).
- [9] A. Stulov, "Hysteretic model of the grand piano hammer felt," *J. Acoust. Soc. Am.* **97**, 2577-2585, (1995).
- [10] A. Stulov and A. Mägi, "Piano hammer: Theory and experiment," *Proc. of the International Symposium on Musical Acoustics (ISMA'2001)*, September 10-14, 2001 Perugia, Italy, Vol. 1, 215-220, (2001).
- [11] A. Stulov, "Comparison of string vibration spectra excited by a different piano hammers," *Proc. Institute of Acoustics, ISMA'97*, Vol. 19: Part 5, Book 1, 231-238, (1997).
- [12] A. Stulov and A. Mägi, "Piano hammer testing device," *Proc. Estonian Acad. Sci. Engin.* **6**, 259-267, (2000).
- [13] Lawson, C. L. & R. J. Hanson, R. J., *Solving least-squares problems*, Prentice-Hall (Englewood Cliffs, N. J., 1974).